Electronic Supplementary Material (ESI) for Physical Chemistry Chemical Physics.

Supporting information for

Validating Experiments for the Reaction $H_2 + NH_2^-$ by Dynamical Computations on an Accurate Full-Dimensional Potential Energy Surface

Kaisheng Song,[1] Hongwei Song,[2,*] and Jun Li[1,*]

[1] *School of Chemistry and Chemical Engineering & Chongqing Key Laboratory of Theoretical and Computational Chemistry, Chongqing University, Chongqing 401331, P.R. China*

[2] *State Key Laboratory of Magnetic Resonance and Atomic and Molecular Physics, Wuhan Institute of Physics and Mathematics, Innovation Academy for Precision Measurement Science and Technology, Chinese Academy of Sciences, Wuhan 430071, China*

*: *Corresponding authors, emails:* hwsong@wipm.ac.cn (HS) and jli15@cqu.edu.cn (JL).

SI. Fitting the PES

98 154 points were fitted by the following neural network (NN) with two hidden layers.[1, 2]

$$V = b_1^{(3)} + \sum_{k=1}^{K}\left(\omega_{1,k}^{(3)} \cdot f_2\left(b_k^{(2)} + \sum_{j=1}^{J}\left(\omega_{k,j}^{(2)} \cdot f_1\left(b_j^{(1)} + \sum_{i=1}^{I} \omega_{j,i}^{(1)} \cdot G_i \right)\right)\right)\right), \quad (1)$$

$$G_i = \hat{S}\prod_{i<j}^{N} p_{ij}^{l_{ij}} , \quad (2)$$

To ensure permutation symmetry,[2, 3] 207 PIPs (G_i, i=1, I, I=207) up to 5th order were used in the input layer of NN. Explicitly, $p_{ij} = \exp(-\lambda r_{ij})$ with r_{ij} being internuclear distances between atoms i and j (i, j = 1–5),[4] and λ an adjusted parameter. In this work, λ is set as 2.1 Å^{-1} so that the PES can well describe the long-range interaction in the reactant and product channels. The symmetrization operator $\hat{S}$ contains all 24 permutations among the four identical hydrogen atoms (4!=24). J and K are the numbers of neurons in the two hidden layers and f_i (i = 1, 2) are nonlinear transfer functions for the two hidden layers. $\omega_{j,i}^{(l)}$ are weights that connect the ith neuron of (l-1)th layer and the jth neuron of the lth layer. $b_j^{(l)}$ are the bias of the jth neuron of the lth layer.

After testing, J and K were chosen to be 15 and 80, respectively, yielding 4481 fitting parameters for each PIP-NN potential. For each NN architecture, the fitting parameters ω and b were determined by minimizing the root-mean-square error (RMSE),

$$\text{RMSE}=\sqrt{\sum_{i=1}^{N_{\text{data}}}\left(E_{\text{output}}^{i} - E_{\text{target}}^{i}\right)^2 / N_{\text{data}}} . \quad (3)$$

To avoid the so called “over-fitting” issue, the dataset was randomly divided into three parts: the training (90%), validation (5%), and test (5%) sets. Besides, for each NN architecture, 100~200 NN trainings with different initial parameters and different training, validation, and test sets were performed.

SII. Quasi-classical trajectory (QCT) calculation details

1) QCT kinetics

Using the newly fitted PES, we carried out kinetics computations by the QCT method as implemented in the VENUS dynamical code.[5] Thermal rate coefficients of R1 in the forward direction at temperatures of 50, 100, 150, 200 and 300 K were calculated according to the following formula:

$$k(T) = \sqrt{\left(\frac{8k_B T}{\pi\mu}\right)}\pi b_{max}^2 \frac{N_r}{N_{tot}}, \quad (4)$$

where T is the temperature, k_B the Boltzmann constant, μ the reactant's reduced mass. At the specified initial temperature, N_r is the number of reactive trajectories taking place out of N_{tot} trajectories. The maximal impact parameter b_{max} is determined with trial values at each specified initial state. Then for each initial state, the impact parameter b is sampled by $b = RN^{1/2}b_{max}$, where RN is a uniform random number in [0, 1]. Other scattering parameters, such as the mutual orientation between initial reactants and vibrational phases, were sampled using the Monte Carlo approach.[6] Initially, the reactants were separated by 26.5 Å. The trajectory was terminated when the products or reactants were separated by 26.5 Å and 27.5 Å for reactive trajectories and non-reactive trajectories, respectively. The initial and termination criteria are much larger than those in the neutral-neutral molecular reactions due to long-range interactions in the ion-molecule reactions. The gradients of the PES with respect to atomic coordinates were determined numerically by a central difference algorithm. The combined fourth-order Runge-Kutta and sixth-order Adams-Moulton algorithms[7] were adopted for the integration of the trajectories with a time step of 0.05 fs. Nearly all trajectories conserved energy within 10^{-3} kcal mol^{-1}, validating the smoothness of the PES.

2) QCT dynamics

For reactions H_2 (j=0, 1, 2) + NH_2^- → H^- + NH_3, the corresponding integral cross section (ICS) was calculated by

$$\sigma_r(E_c, j_{H_2}) = \pi b_{max}^2(E_c, j_{H_2}) P_r(E_c, j_{H_2}) \quad (5)$$

where $P_r(E_c, j_{H2})$ is the reaction probability and defined as the ratio between the number of reactive (N_r) and total (N_{tot}) trajectories at a specified collision energy E_c and H_2 rotational state. The statistical

error was measured by $\Delta = \sqrt{(N_{\text{tot}} - N_{\text{r}}) / (N_{\text{tot}} N_{\text{r}})}$.

The differential cross section (DCS) was computed by

$$\frac{d\sigma_{\text{r}}}{d\Omega} = \frac{\sigma_{\text{r}} Q_{\text{r}}(\theta)}{2\pi \sin(\theta)} \tag{6}$$

where $Q_{\text{r}}(\theta)$ is the normalized angular distribution with the scattering angle, θ, defined as

$$\theta = \cos^{-1}\left(\frac{\vec{v}_i \bullet \vec{v}_f}{|\vec{v}_i||\vec{v}_f|} \right) \tag{7}$$

Here, $\vec{v}_i = \vec{v}_{\text{H}_2} - \vec{v}_{\text{NH}_2^-}$ and $\vec{v}_f = \vec{v}_{\text{H}^-} - \vec{v}_{\text{NH}_3}$ denote the relative velocity vector for initial and final positions, respectively. Thus, trajectories with θ = 0° and θ = 180° correspond to the forward and backward scattering, respectively.

3) Reaction channels

Theoretically, there exist 4 pathways, R1a, R1b, R1c and R1d, for the abstraction reaction R1. Namely,

$$H_1H_2 + H_3NH_4^- \leftrightarrow H_1^- + NH_2H_3H_4 \qquad \text{R1a}$$

$$H_1H_2 + H_3NH_4^- \leftrightarrow H_2^- + NH_1H_3H_4 \qquad \text{R1b}$$

$$H_1H_2 + H_3NH_4^- \leftrightarrow H_3^- + NH_1H_2H_4 \qquad \text{R1c}$$

$$H_1H_2 + H_3NH_4^- \leftrightarrow H_4^- + NH_1H_2H_3 \qquad \text{R1d}$$

Note that the subscripts in H_1H_2 and $H_3NH_4^-$ are for the numbering of the hydrogen atoms. R1a and R1b are the main pathways. The reaction probabilities of R1c and R1d are very low and can be neglected.

In order to have a better understanding of the reaction mechanisms of R1 reaction, 6 trajectory animations are provided. Two animations, Traj-1 and Traj-2, clarify the direct striping and rebound mechanism, respectively. Traj-3 and Traj-4 clarify the indirect reaction mechanism. In Traj-3, when $H_3NH_4^-$ captures H_1, H_2^- does not leave immediately, but keeps rotating around $NH_1H_3H_4$ for a long time before moving away. In Traj-4, similar to but different from Traj-3, H_2H_1 is generated by taking away H_1 from $NH_1H_3H_4$ at some point during the rotation of H_2^- around $NH_1H_3H_4$, and then H_1 from

H_2H_1 is taken away by $NH_3H_4^-$. Traj-5 and Traj-6 represent R1c and R1d, respectively. Traj-5 is similar to Traj-4, H_2H_3 is generated by taking away H_3 from $NH_1H_3H_4$, and then H_2 from H_2H_3 is taking away by $NH_1H_4^-$. Traj-6 is more complex than Traj-5, H_1H_2 is generated by taking away H_1 from $NH_1H_3H_4$, and then H_1 from H_1H_2 is taking away by $NH_3H_4^-$. Again, H_2H_4 is generated by taking away H_4 from $NH_1H_3H_4$, and finally H_2 from H_2H_4 is taking away by $NH_1H_3^-$.

SIII. Quantum dynamics

The initial state-selected time-dependent wave packet approach has been well documented in the literature.[8] We introduce briefly here the model relevant to this work. For the diatom-triatom reaction, the full-dimensional Hamiltonian in the reactant Jacobi coordinates, as shown below,

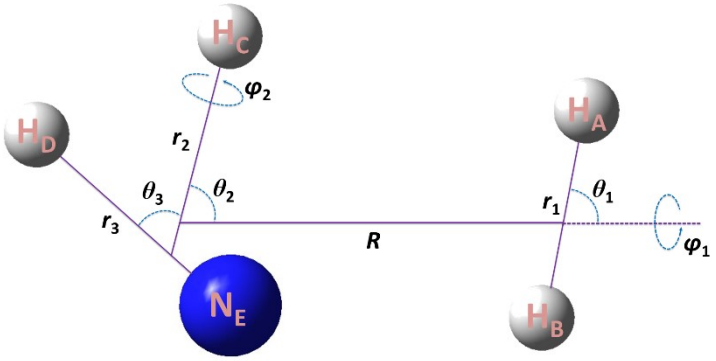

The full-dimensional Jacobi coordinates used for the diatom-triatom collision system.

is defined as ($\hbar = 1$ hereafter)[9-11]

$$\hat{H} = -\frac{1}{2\mu_R}\frac{\partial^2}{\partial R^2} - \frac{1}{2\mu_1}\frac{\partial^2}{\partial r_1^2} - \frac{1}{2\mu_2}\frac{\partial^2}{\partial r_2^2} - \frac{1}{2\mu_3}\frac{\partial^2}{\partial r_3^2} + \frac{(\hat{J}_{tot} - \hat{J})^2}{2\mu_R R^2} + \frac{\hat{j}_1^2}{2\mu_1 r_1^2} + \frac{\hat{l}_2^2}{2\mu_2 r_2^2} + \frac{\hat{j}_3^2}{2\mu_3 r_3^2} + \hat{V}(R, r_1, r_2, r_3, \theta_1, \theta_2, \theta_3, \varphi_1, \varphi_2) \quad (8)$$

where R, r_1, r_2 and r_3 are the radial coordinates. μ_R, μ_1, μ_2, and μ_3 denote the corresponding reduced masses. $\hat{j}_3$ represents the rotational angular momentum operator of H_DN_E and $\hat{l}_2$ refers to the orbital angular momentum operator of H_C with respect to H_DN_E. $\hat{j}_{23}$ denotes the coupling of $\hat{l}_2$ and $\hat{j}_3$. $\hat{j}_1$ is the rotational angular momentum operator of H_AH_B. $\hat{J}$ denotes the coupling of $\hat{j}_1$ and $\hat{j}_{23}$. Since the bond distance of NH in NH_2 changes slightly along the MEP on the PES, less than 0.02 a_0, the two bonds are expected to behave as a spectator bond in the reaction. To reduce the computational costs, r_2 and

r_3 are fixed at 1.975 and 1.945 a_0, respectively. As a result, the terms $-\frac{1}{2\mu_2}\frac{\partial^2}{\partial r_2^2}$ and $\frac{1}{2\mu_3}\frac{\partial^2}{\partial r_3^2}$ in Eq. (8) are vanished and the full-dimensional model is reduced into a seven-dimensional model.

The parity (ε) adapted wave function of the system is expressed as

$$\psi^{J_{tot}M\varepsilon}(\vec{R},\vec{r}_1,\vec{r}_2,\vec{r}_3) = \sum_{n,v,j,K} F^{J_{tot}M\varepsilon}_{nvjK}\, u^{v_1}_n(R)\phi_{v1}(r_1)\Phi^{J_{tot}M\varepsilon}_{jK}(\hat{R},\hat{r}_1,\hat{r}_2,\hat{r}_3) \tag{9}$$

where the symbol n labels the translational basis functions along the scattering coordinate R, v_1 labels the vibrational basis functions along the coordinate r_1, j represents the composite rotational indices (j_1,l_2,j_3,j_{23},J). The translational basis function, $u^{v_1}_n$, that is related to v_1 due to the employment of an L-shaped grid in the calculations,[12] is taken as the sine functions. The vibrational basis function, ϕ_{v1}, is obtained by solving one-dimensional reference Hamiltonian. The eigenfunction of the parity(ε)-adapted coupled body-fixed (BF) total angular momentum, $\Phi^{J_{tot}M\varepsilon}_{jK}$, is defined as

$$\Phi^{J_{tot}M\varepsilon}_{jK} = (1+\delta_{K0})^{-1/2}\sqrt{\frac{2J_{tot}+1}{8\pi}}[D^{J_{tot}*}_{K,M} Y^{JK}_{j_1j_{23}l_2j_3} + \varepsilon(-1)^{j_1+l_2+j_3+J+J_{tot}} D^{J_{tot}*}_{-K,M} Y^{J-K}_{j_1j_{23}l_2j_3}], \tag{10}$$

where $D^J_{K,M}$ is the Wigner rotation matrix.[13] M and K are the projections of the total angular momentum on the space-fixed and BF z axes. The BF z axis is defined along the Jacobi coordinate R. $Y^{JK}_{j_1j_{23}l_2j_3}$ denotes the eigenfunction of the coupled angular momentum operator $\hat{J}$.

The centrifugal sudden approximation,[14, 15] namely neglecting the coupling between different K blocks, is implemented in the calculations. The second-order split-operator method is employed to propagate the wave packet.[16] To prevent artificial boundary reflections, the damping function, defined as $D(x) = -i\alpha(\frac{x-x_s}{x_{max}-x_s})^n$, is used at the grid edges. The initial wave packet is damped after 400 steps from x_s along the radial coordinates R and r_1. The initial state-specific total reaction probability is computed by the flux operator approach.[17] Since this work focuses on the reactant rotational effect, the reactants H_2 and NH_2^- are both launched from the ground vibrational states.

The numerical parameters are listed in Table S2, which are carefully tested to give converged dynamical results. For the scattering coordinate R, 155 sine discrete variable representation (DVR)

basis functions/grid points are used in the whole range from 1.4 to 20.0 a_0 and 31 of them are used to define the interaction region. For the radial coordinate r_1, 25 potential optimized DVR (PODVR) basis functions/grid points are employed in the interaction region defined from 0.7 to 6.5 a_0 and 3 in the asymptotic region. The size of rotational basis is determined by $j_{1\max} = 31$, $l_{2\max} = 24$, $j_{3\max} = 20$, $j_{23\max} = 20$ and $J_{\max} = 40$, giving a total of 1 703 982 rotational bases. The initial wave packet is propagated by around 50 000 *a.u.* with a time step of 10 *a.u.*

SIV. Figures

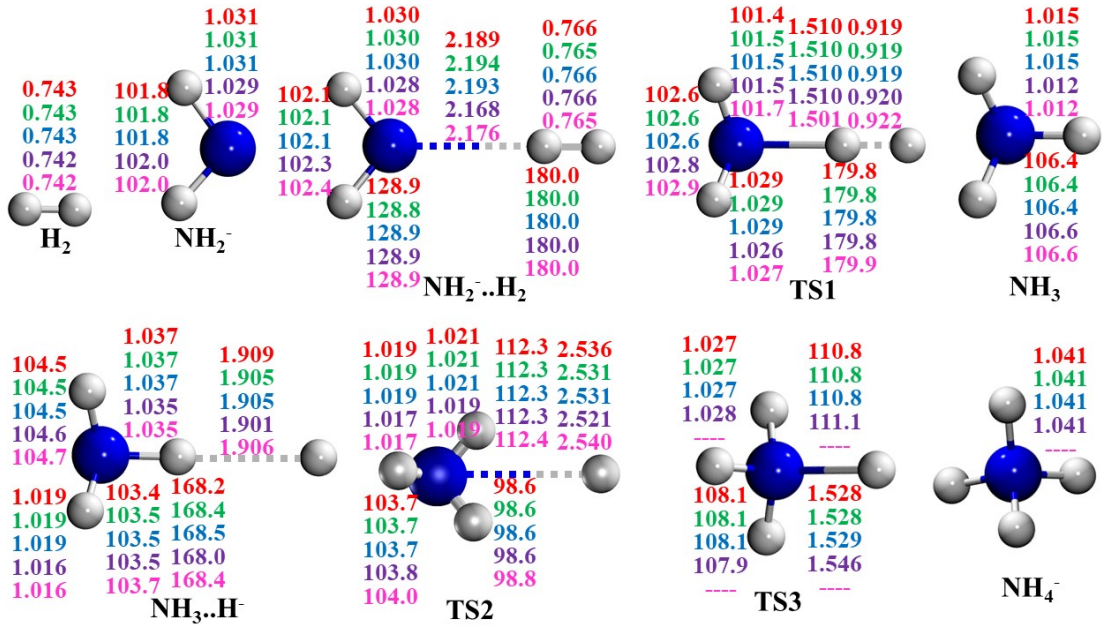

Fig. S1 Geometries of the stationary and points (angles in ° and distances in Å) at various levels: PIP-NN PES, UCCSD(T)/AVTZ′, CCSD(T)/AVTZ′, CCSD(T)-F12a/AVTZ, FI-NN PES,[18] from top to bottom.

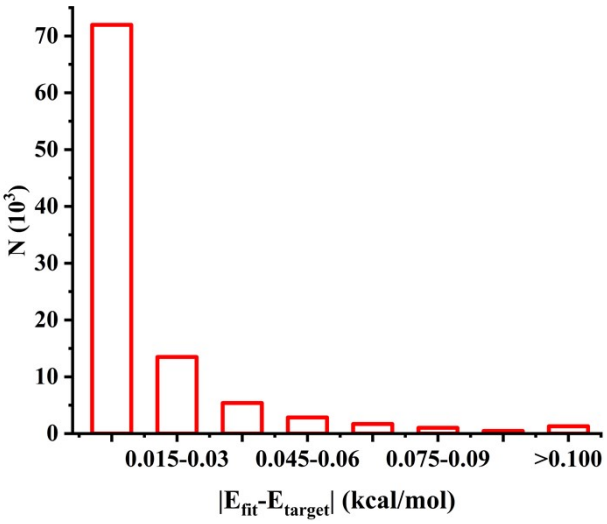

Fig. S2 Distribution of the unsigned fitting errors for the fitted points.

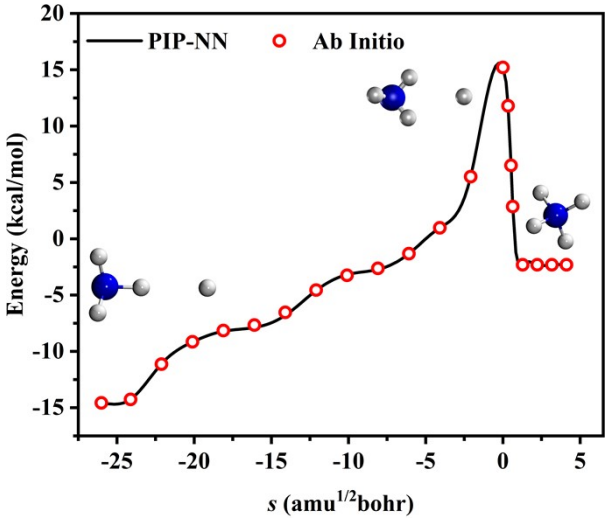

Fig. S3 Potential energies along the MEPs for the process between $NH_3 \cdots H^-$ and NH_4^- as a function of the reaction coordinate *s* (amu$^{1/2}$bohr).

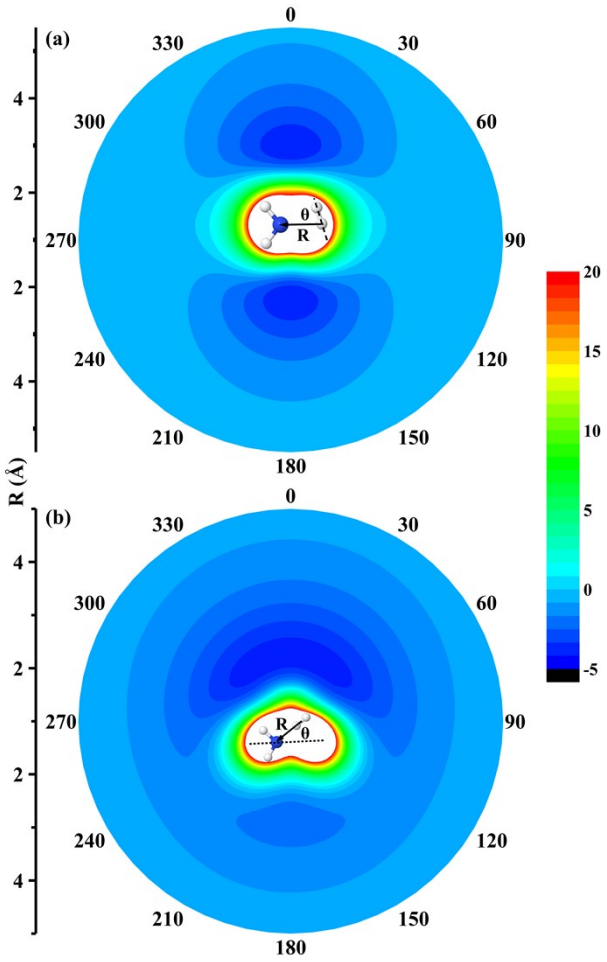

Fig. S4 Polar contours of the potential energy for the NH_2^- + H_2 system as a function of θ and $R_{NH'}$ (a) or R (the distance between N and the centroid of H_2) (R in Å and θ in °). Both NH_2^- and H_2 are fixed at the equilibrium.

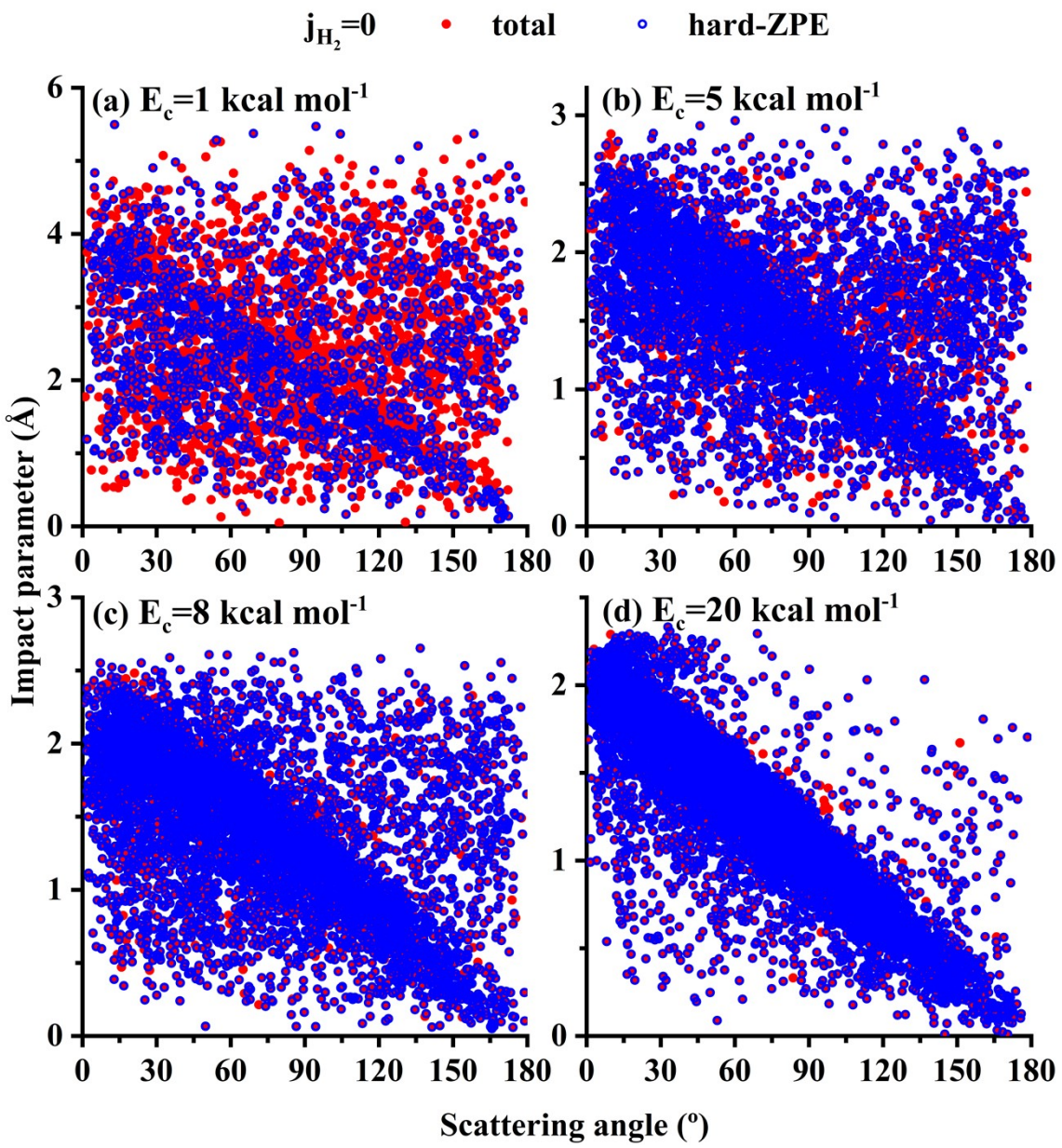

Fig S5. Correlations between the impact parameter and the scattering angle for the NH_2^- + H_2 (j=0) → NH_3 + H^- reaction at E_c = 1, 5, 8, 10 kcal mol^{-1}, respectively.

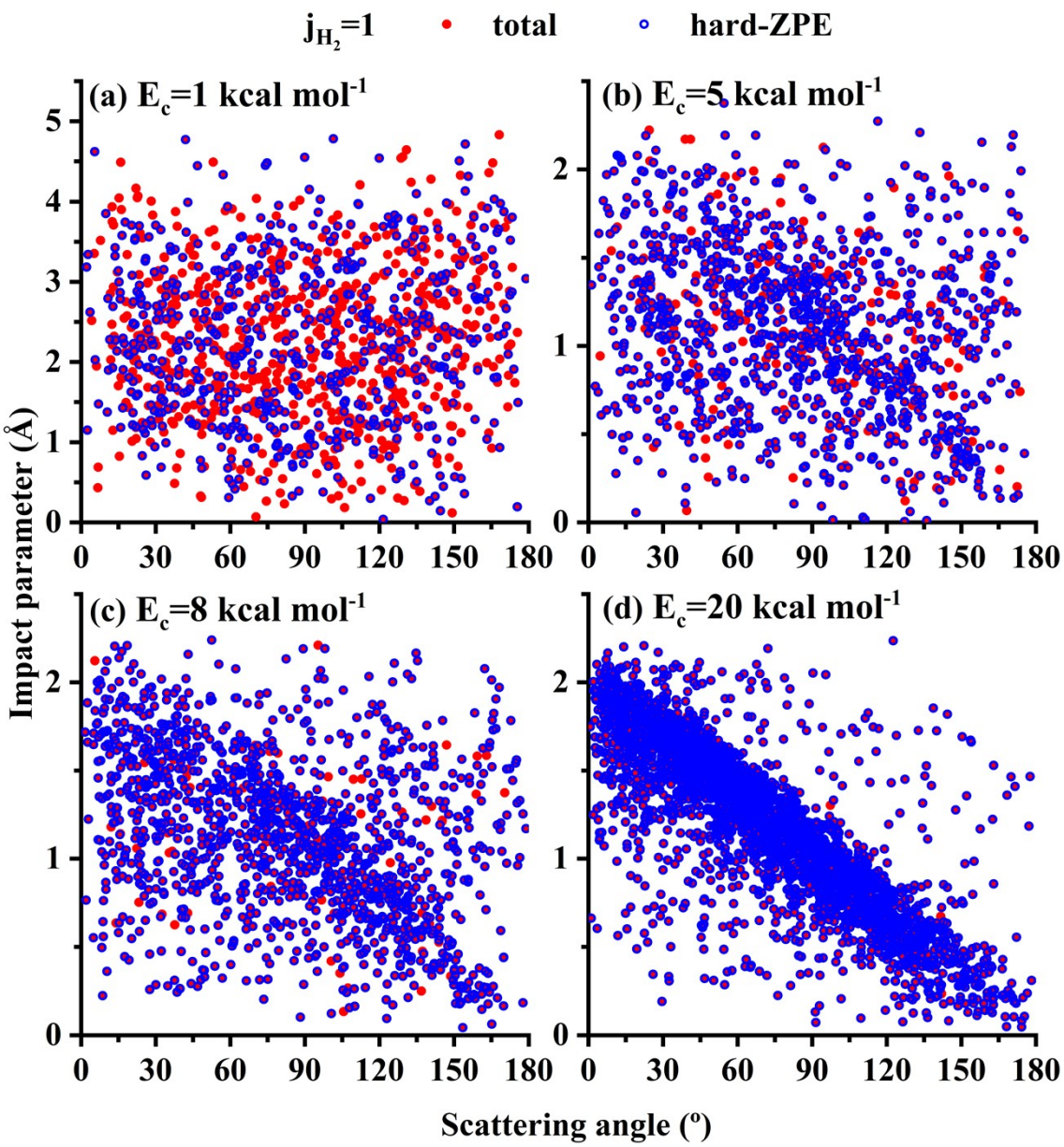

Fig. S6 Correlations between the impact parameter and the scattering angle for the NH_2^- + H_2 (j=1) → NH_3 + H^- reaction at E_c = 1, 5, 8, 10 kcal mol^{-1}, respectively.

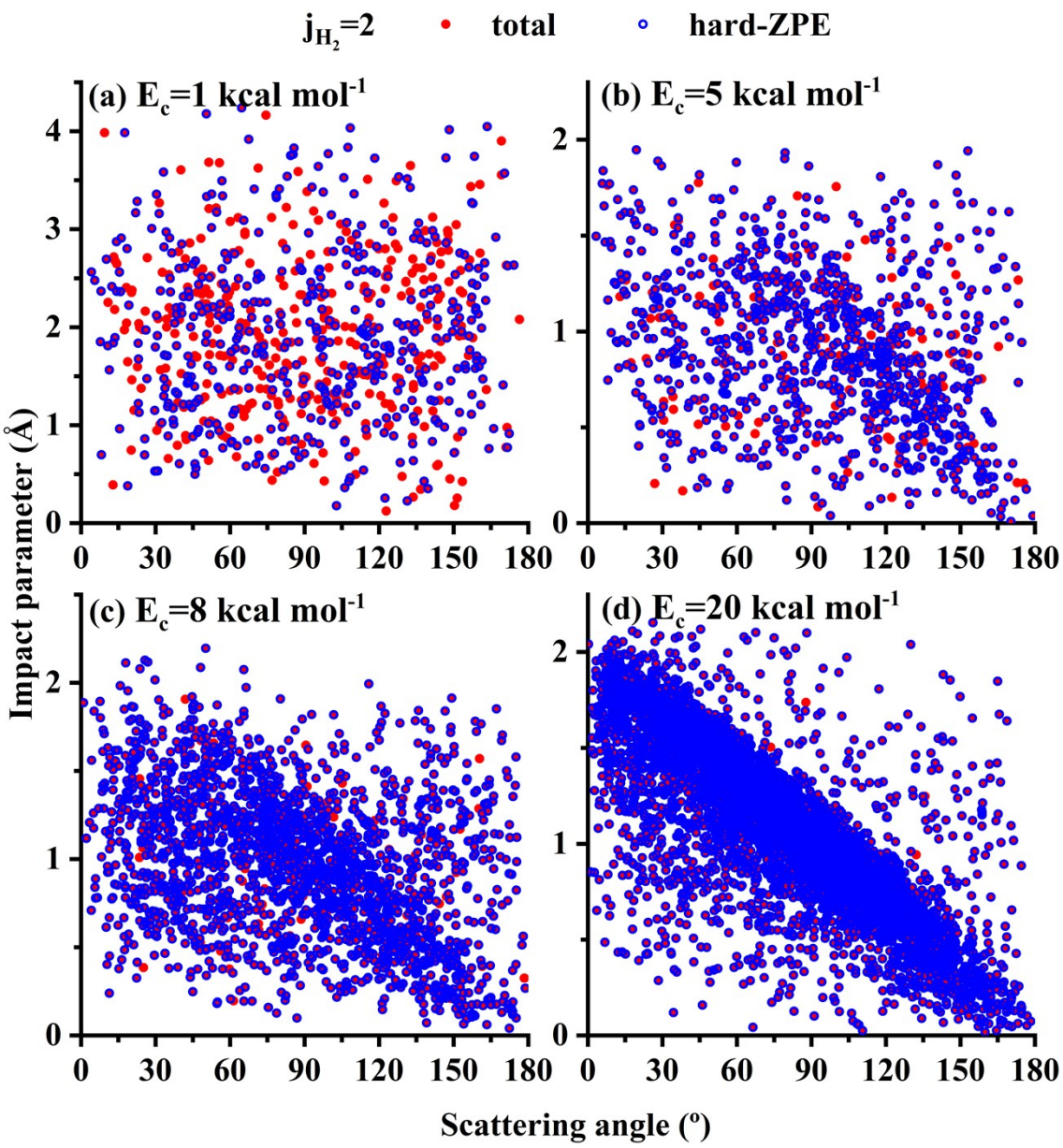

Fig. S7 Correlations between the impact parameter and the scattering angle for the NH_2^- + H_2 (j=2) → NH_3 + H^- reaction at E_c = 1, 5, 8, 10 kcal mol^{-1}, respectively.

SV. Tables

Table S1. Harmonic frequencies (cm^{-1}) of the stationary points at various levels along the $H_2 + NH_2^- \rightarrow H^- + NH_3$ reaction system.

Species	Note	Frequency (cm^{-1})								
		1	2	3	4	5	6	7	8	9
$H_2 + NH_2^-$	PIP-NN PES[a]	4398.5	1488.5	3279.7	3363.2					
	Ab initio[b]	4400.2	1486.6	3279.1	3363.0					
	Ab initio[c]	4400.2	1488.0	3279.5	3363.0					
	Ab initio[d]	4400.5	1488.8	3292.7	3377.4					
	FI-NN PES[e]	4398.0	1484.0	3293.0	3388.0					
$H_2 \cdots NH_2^-$	PIP-NN PES[a]	131.0	286.0	688.3	753.0	1498.7	3293.2	3378.5	3989.4	35.7i
	Ab initio[b]	140.6	284.1	688.7	755.4	1494.1	3288.5	3372.5	3993.5	28.5i
	Ab initio[c]	140.0	283.5	690.8	757.1	1494.0	3288.8	3372.5	3990.4	49.9i
	Ab initio[d]	124.0	289.9	693.3	775.7	1494.7	3303.5	3388.9	3967.0	61.9i
	FI-NN PES[e]	141.0	295.0	707.0	752.0	1495.0	3306.0	3399.0	4005.0	74.0
TS1	PIP-NN PES[a]	372.2	409.7	1276.9	1384.2	1510.9	1857.8	3305.8	3400.4	853.9i
	Ab initio[b]	371.0	420.0	1286.0	1404.0	1508.0	1821.0	3314.0	3429.0	881.0i
	Ab initio[c]	369.3	406.2	1279.0	1385.5	1508.5	1854.6	3309.5	3399.0	853.8i
	Ab initio[d]	370.7	406.3	1282.9	1392.8	1510.5	1848.7	3325.9	3416.7	854.1i
	FI-NN PES[e]	373.2	408.4	1283.7	1393.2	1510.8	1848.7	3326.1	3416.9	853.6i

$NH_3…H^-$	PIP-NN PES[a]	310.2	384.4	424.7	1215.3	1651.9	1693.3	3171.8	3462.3	3531.2
	Ab initio[b]	310.1	382.7	419.5	1211.6	1653.4	1695.7	3169.8	3459.2	3531.7
	Ab initio[c]	309.4	383.0	421.0	1211.6	1653.8	1695.6	3169.8	3459.9	3532.1
	Ab initio[d]	309.2	384.4	423.7	1213.7	1655.5	1698.5	3175.5	3474.4	3548.2
	FI-NN PES[e]	306.0	391.0	418.0	1206.0	1640.0	1694.0	3164.0	3487.0	3544.0
$H^- + NH_3$	PIP-NN PES[a]	1063.1	1670.8	1671.0	3464.0	3592.5	3592.5			
	Ab initio[b]	1063.3	1672.6	1673.1	3464.5	3592.2	3592.5			
	Ab initio[c]	1063.5	1672.8	1672.0	3463.9	3592.4	3592.7			
	Ab initio[d]	1054.8	1672.8	1673.0	3477.1	3608.5	3608.6			
	FI-NN PES[e]	1064.0	1675.0	1675.0	3458.0	3606.0	3606.0			
TS2	PIP-NN PES[a]	230.4	336.0	1237.4	1661.5	1666.2	3421.0	3489.0	3529.4	277.6i
	Ab initio[b]	216.3	322.4	1229.4	1660.4	1663.7	3416.6	3484.3	3525.6	290.4i
	Ab initio[c]	232.4	332.2	1230.8	1662.5	1665.5	3416.7	3485.4	3526.0	274.6i
	Ab initio[d]	233.7	334.7	1235.1	1663.8	1670.3	3428.2	3497.0	3540.7	279.1i
	FI-NN PES[e]	253.0	345.0	1231.0	1655.0	1676.0	3426.0	3495.0	3540.0	251.0i
TS3	PIP-NN PES[a]	490.5	491.9	1100.8	1602.3	1602.4	3205.3	3437.2	3437.4	1296.2i
	Ab initio[b]	500.5	504.0	1101.2	1604.1	1606.0	3220.5	3434.7	3439.2	1289.3i
	Ab initio[c]	469.1	482.5	1098.8	1594.8	1597.7	3211.1	3432.5	3434.5	1302.9i
	Ab initio[d]	452.5	455.1	1086.3	1585.5	1586.0	3186.4	3399.4	3399.7	1247.4i
NH_4^-	PIP-NN PES[a]	1343.7	1344.1	1344.9	1610.9	1611.4	3010.7	3101.7	3102.0	3102.2
	Ab initio[b]	1344.5	1345.0	1345.2	1619.3	1619.4	3012.6	3117.2	3117.5	3117.6

	Ab initio[c]	1344.9	1345.0	1345.8	1619.1	1620.4	3013.3	3117.1	3117.5	3117.9
	Ab initio[d]	1332.9	1333.0	1333.1	1605.3	1605.5	2990.1	3099.5	3099.5	3099.6

[a] PIP-NN PES, this work; [b] UCCSD(T)/AVTZ′, this work; [c] CCSD(T)/AVTZ′, this work; [d] CCSD(T)-F12a/AVTZ, this work; [e] FI-NN PES.[18]

Table S2. Numerical parameters used in the quantum dynamics calculations (unless otherwise stated, atomic units are used).

$H_2 + NH_2^- \rightarrow H^- + NH_3$	
Grid/basis range and size:	$R \in [1.4, 20.0]$ $N_R^{tot} = 155, N_R^{int} = 31$ $r_1 \in [0.7, 6.5]$ $N_{r_1}^{int} = 25, N_{r_1}^{asy} = 3$ $j_{1max} = 30, j_{23max} = 20, j_{3max} = 20$ $l_{2max} = 24, J_{max} = 40$
Initial wave packet:	$R_0 = 15.0, \delta = 0.35, E_i = 0.2\ eV$
Damping term:	$R_a = 15.0, \alpha_R = 0.05, n_R = 2.5$ $r_{2a} = 4.7, \alpha_{r_2} = 0.035, n_{r_2} = 2.0$
Flux position:	$r_2^F = 4.5$

References

1. B. Jiang and H. Guo, *J. Chem. Phys.*, 2013, **139**, 054112.
2. J. Li, B. Jiang and H. Guo, *J. Chem. Phys.*, 2013, **139**, 204103.
3. D. Lu and J. Li, *J. Chem. Phys.*, 2016, **145**, 014303.
4. Z. Xie and J. M. Bowman, *J. Chem. Theory Comput.*, 2010, **6**, 26-34.
5. W. L. Hase, R. J. Duchovic, X. Hu, A. Komornicki, K. F. Lim, D.-H. Lu, G. H. Peslherbe, K. N. Swamy, S. R. V. Linde, A. Varandas, H. Wang and R. J. Wolf, *Quantum Chemistry Program Exchange Bulletin*, 1996, **16**, 671.
6. X. Hu, W. L. Hase and T. Pirraglia, *J. Comput. Chem.*, 1991, **12**, 1014.
7. D. L. Bunker, *Meth. Comp. Phys.*, 1971, **10**, 287-325.
8. J. Z. H. Zhang, *Theory and Application of Quantum Molecular Dynamics*, World Scientific, Singapore, 1999.
9. D. Wang, *J. Chem. Phys.*, 2006, **124**, 201105.
10. M. Yang, *J. Chem. Phys.*, 2008, **129**, 064315.
11. H. Song, J. Li, M. Yang, Y. Lu and H. Guo, *Phys. Chem. Chem. Phys.*, 2014, **16**, 17770-17776.
12. D. H. Zhang and J. Z. H. Zhang, *J. Chem. Phys.*, 1993, **99**, 5615.
13. R. N. Zare, *Angular Momentum*, John Wiley & Sons, Inc., New York, 1988.
14. R. T. Pack, *J. Chem. Phys.*, 1974, **60**, 633-639.
15. P. McGuire and D. J. Kouri, *J. Chem. Phys.*, 1974, **60**, 2488-2499.
16. J. A. Flect Jr., J. R. Morris and M. D. Feit, *Appl. Phys.*, 1976, **10**, 129.
17. W. H. Miller, S. D. Schwartz and J. W. Tromp, *J. Chem. Phys.*, 1983, **79**, 4889-4899.
18. M. Pan, H. Xiang, Y. Li and H. Song, *Phys. Chem. Chem. Phys.*, 2021, **23**, 17848-17855.